AD-A071 438 LEHIGH UNIV BETHLEHEM PA INST OF FRACTURE AND SOLID --ETC F/G 11/6
FRACTURE MECHANICS AND SURFACE CHEMISTRY STUDIES OF FATIGUE CRA--ETC(U)
APR 79 R P WEI, P S PAO, R G HART, T W WEIR N00014-75-C-0543

UNCLASSIFIED IFSM-79-98 NL

1 OF 1
AD A071438

END
DATE FILMED
8-79
DDC

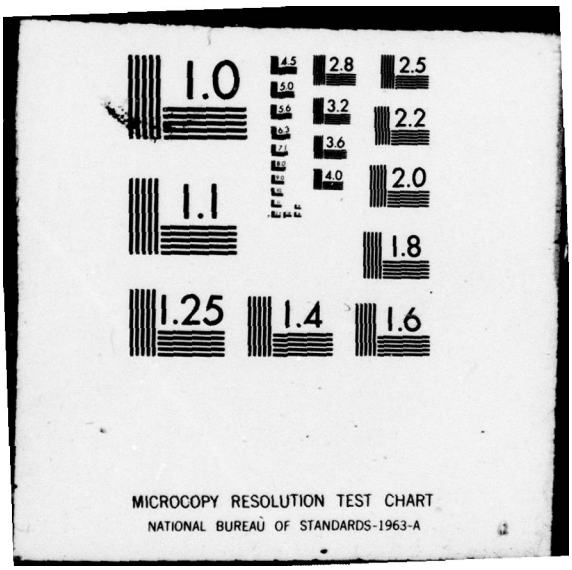
1.0
1.1
1.25
1.4
1.6
1.8
2.0
2.2
2.5
2.8
3.2
3.6
4.0
4.5
5.0
5.6
6.3
MICROCOPY RESOLUTION TEST CHART
NATIONAL BUREAU OF STANDARDS-1963-A

12

IFSM-79-98

LEHIGH UNIVERSITY

LEVEL

FRACTURE MECHANICS AND SURFACE CHEMISTRY STUDIES OF FATIGUE CRACK GROWTH IN AN ALUMINUM ALLOY

by

R. P. Wei, F. S. Pao, R. G. Hart, T. W. Weir and G. W. Simmons

April, 1979

Report No. 9

Office of Naval Research

UNCLASSIFIED

SECURITY CLASSIFICATION OF THIS PAGE (When Data Entered)

(14) **REPORT DOCUMENTATION PAGE**

READ INSTRUCTIONS BEFORE COMPLETING FORM

1. REPORT NUMBER: IFSM-79-98, TR-9	2. GOVT ACCESSION NO.
3. RECIPIENT'S CATALOG NUMBER: (9)	
4. TITLE (and Subtitle): (6) FRACTURE MECHANICS AND SURFACE CHEMISTRY STUDIES OF FATIGUE CRACK GROWTH IN AN ALUMINUM ALLOY.	5. TYPE OF REPORT & PERIOD COVERED: Technical Report, No. 9
	6. PERFORMING ORG. REPORT NUMBER: (15)
7. AUTHOR(s): (10) R. P. Wei, P. S. Pao, R. G. Hart, T. W. Weir and G. W. Simmons	8. CONTRACT OR GRANT NUMBER(s): Contract N00014-75-C-0543
9. PERFORMING ORGANIZATION NAME AND ADDRESS: Lehigh University, Bethlehem, PA 18015	10. PROGRAM ELEMENT, PROJECT, TASK AREA & WORK UNIT NUMBERS: NR 036-097
11. CONTROLLING OFFICE NAME AND ADDRESS: Office of Naval Research, Department of the Navy, Arlington, VA (11)	12. REPORT DATE: April 1979
	13. NUMBER OF PAGES: 29
14. MONITORING AGENCY NAME & ADDRESS(if different from Controlling Office): (12) 36p.	15. SECURITY CLASS. (of this report): Unclassified
	15a. DECLASSIFICATION/DOWNGRADING SCHEDULE

16. DISTRIBUTION STATEMENT (of this Report)

This document has been approved for public release and sale; its distribution is unlimited.

17. DISTRIBUTION STATEMENT (of the abstract entered in Block 20, if different from Report)

18. SUPPLEMENTARY NOTES

19. KEY WORDS (Continue on reverse side if necessary and identify by block number)

Fracture Mechanics, Surface Chemistry, Corrosion Fatigue, Hydrogen Embrittlement, Aluminum Alloy, Water-Metal Reactions

20. ABSTRACT (Continue on reverse side if necessary and identify by block number)

Fracture mechanics and surface chemistry studies were carried out to develop further understanding of the influence of water vapor on fatigue crack growth in aluminum alloys. The room temperature fatigue crack growth response was determined for 2219-T851 aluminum alloy exposed to water vapor at pressures from 1 Pa to 30 Pa over a range of stress intensity factors (K). Data were also obtained in vacuum (at < 0.50 μPa), and dehumidified argon. The test results showed that, at a frequency of 5 Hz, the rate of crack growth is

DD FORM 1 JAN 73 1473 EDITION OF 1 NOV 65 IS OBSOLETE S/N 0102-014-6601

UNCLASSIFIED

SECURITY CLASSIFICATION OF THIS PAGE (When Data Entered)

407099

79 07 19 013

essentially unaffected by water vapor until a threshold pressure is reached. Above this threshold, the rates increased, reaching a maximum within one order of magnitude increase in vapor pressure. This maximum crack growth rate is equal to that obtained in air (40 to 60 pct relative humidity), distilled water and 3.5 pct NaCl solution on the same material. Parallel studies of the reactions of water vapor with fresh alloy surfaces (produced either by in situ impact fracture or by ion etching) were made by Auger electron spectroscopy (AES) and x-ray photoelectron spectroscopy (XPS). The extent of surface reaction was monitored by changes in the oxygen AES and XPS signals.

Correlation between the fatigue crack growth response and the surface reaction kinetics has been made, and is consistent with a transport-limited model for crack growth. The results also suggest that enhancement of fatigue crack growth by water vapor in the aluminum alloys occurs through a "hydrogen embrittlement" mechanism.

FRACTURE MECHANICS AND SURFACE CHEMISTRY STUDIES OF FATIGUE CRACK GROWTH IN AN ALUMINUM ALLOY

by

R. P. Wei, P. S. Pao*, R. G. Hart,
T. W. Weir and G. W. Simmons
LEHIGH UNIVERSITY
Bethlehem, PA 18015

*Present address: McDonnell Douglas Research Laboratory, St. Louis, MO 63166

FRACTURE MECHANICS AND SURFACE CHEMISTRY STUDIES OF FATIGUE CRACK GROWTH IN AN ALUMINUM ALLOY

R. P. Wei, P. S. Pao*, R. G. Hart,
T. W. Weir and G. W. Simmons
LEHIGH UNIVERSITY
Bethlehem, PA 18015

ABSTRACT

Fracture mechanics and surface chemistry studies were carried out to develop further understanding of the influence of water vapor on fatigue crack growth in aluminum alloys. The room temperature fatigue crack growth response was determined for 2219-T851 aluminum alloy exposed to water vapor at pressures from 1 Pa to 30 Pa over a range of stress intensity factors (K). Data were also obtained in vacuum (at < 0.50 μPa), and dehumidified argon. The test results showed that, at a frequency of 5 Hz, the rate of crack growth is essentially unaffected by water vapor until a threshold pressure is reached. Above this threshold, the rates increased, reaching a maximum within one order of magnitude increase in vapor pressure. This maximum crack growth rate is equal to that obtained in air (40 to 60 pct relative humidity), distilled water and 3.5 pct NaCl solution on the same material. Parallel studies of the reactions of water vapor with fresh alloy surfaces (produced either by in situ impact fracture or by ion etching) were made by Auger electron spectroscopy (AES) and x-ray photoelectron spectroscopy (XPS). The extent of surface reaction was monitored by changes in the oxygen AES and XPS signals

Correlation between the fatigue crack growth response and the surface reaction kinetics has been made, and is consistent with a transport-limited model for crack growth. The results also suggest that enhancement of fatigue crack growth by water vapor in the aluminum alloys occurs through a "hydrogen embrittlement" mechanism.

*Present address: McDonnell Douglas Research Laboratory, St. Louis, MO 63166

INTRODUCTION

The influences of cyclic load frequency and gas pressure on environment assisted fatigue crack growth in high-strength alloys has been under study for many years [1-14]. A complete quantitative explanation of this effect and of the differences in response for different alloy-environment combinations is not yet available. To assist in understanding the influences of these variables, coordinated fracture mechanics and surface chemistry studies have been undertaken to identify the rate controlling processes for crack growth in high-strength steels and to assess the roles of these processes in determining environment assisted fatigue crack growth response [15-17]. In the present study, the role of water vapor-metal reaction in determining the crack growth response of aluminum alloys was examined.

Previous studies [6,7] have shown that the rate of fatigue crack growth in aluminum alloys exposed to water vapor (in the absence of capillary condensation at the crack tip) was significantly affected by pressure and frequency. Bradshaw and Wheeler showed that the rate of fatigue crack growth at a given K level appeared to depend on the product of water vapor pressure and cyclic load period (1/frequency), and suggested that the observed frequency effect resulted from the time available for the reaction of water vapor with the newly created crack surfaces [6]. In distilled water, on the other hand, aluminum alloys exhibited little or no effect of frequency [1,8]. Comparable effects of frequency have been reported for fatigue crack growth in high-strength steels, at K levels below K_{Iscc} (the stress corrosion cracking threshold). Barsom [11] showed that the rate of fatigue crack growth in a 12Ni-5Cr-3Mo steel, tested in 3.5 pct NaCl solution at room temperature, depended on cyclic load frequency, with higher growth rates at the lower frequencies. The influence of frequency has also been reported by Gallagher [12] for a HY-80 steel tested in 3.5 pct

NaCl solution, by Miller et al. [13] for a low-alloy steel tested in distilled water, and by Hutin [14] for another low-alloy steel tested in water vapor (without capillary condensation at the crack tip). The frequency effects in steels, however, are observed at lower frequencies, and at higher water vapor pressures (and in aqueous environments) as compared to those in the aluminum alloys. Hudak and Wei [9] suggested that these differences in behavior between steels and aluminum alloys may be attributed to differences in the reactivity of these alloys to water/water vapor. Unfortunately, however, this suggestion could not be assessed at the time because of the lack of relevant surface reaction data on these materials, and because the processes controlling crack growth were not well identified and understood.

Recent fracture mechanics and surface chemistry based studies [15,16] showed that sustained-load crack growth in a low-alloy, high-strength steel, in water/water vapor, is controlled by a slow step in the reaction of water with the steel. This reaction step is associated with the nucleation and growth of oxide on the crack surface and the presumed concomitant production of hydrogen. The enhancement of crack growth is attributed to embrittlement by this hydrogen [16]. Extension of these results to the study of environment assisted fatigue crack growth in this steel by water vapor showed that both steady-state and non-steady-state crack growth response can be adequately explained in relation to the kinetics of water vapor-steel surface reactions [17]. Environment enhancement of fatigue crack growth (at K levels below K_{Iscc}) appeared to be proportional to the extent of surface reaction during one load cycle, and to depend on exposure (pressure x time).

To further assess the role of surface reactions in determining environment assisted fatigue crack growth response and to follow up on the suggestion of Bradshaw and Wheeler [6], coordinated fracture mechanics and surface chemistry studies have been carried out on an Al-Cu alloy (2219-T851 aluminum alloy).

Results from these studies are summarized and discussed in terms of a model for crack growth [18].

MATERIAL AND EXPERIMENTAL WORK

Material, Specimen and K Calibration

A 1.65 cm thick plate[1/] of 2219-T851 aluminum alloy was used in this study. Nominal tensile properties of this plate are as follows: yield strength = 358 MPa and tensile strength = 455 MPa.

Wedge-opening-load (WOL) specimens, with half-height to width ratio (H/W) of 0.486, were selected for use. The specimens were oriented in the longitudinal (LT) orientation. An initial (or crack starter) notch, 1.96 cm in length, was introduced into each specimen by electro-discharge machining (EDM). Each specimen was precracked in fatigue, while exposed to the test environment, through a decreasing sequence of loads that terminated at the desired load level (or initial K) for the actual experiment. The precracking procedure provided a fatigue crack of about 0.33 cm in length from the starter notch, corresponding to a crack length of about 2.3 cm at the start of each experiment. This precracking procedure ensured that the subsequent fatigue crack growth would be through material that had not been altered by the notch preparation procedure, and would be unaffected by the starter notch geometry.

Stress intensity factor, K, for the WOL specimen was computed from Eq. 1 [19,20]:

$$K = \frac{P}{BW}\sqrt{a}\,[30.96 - 195.8\,(a/W) + 730.6\,(a/W)^2 - 1186.3\,(a/W)^3 + 754.6\,(a/W)^4] \quad (1)$$

1/Plate furnished by Air Force Flight Dynamics Laboratory, WPAB, OH.

P = applied load; B = specimen thickness; W = specimen width; and a = crack length. Both specimen width and crack length were measured from the line of loading.

Test Environment

Crack growth experiments were carried out in dehumidified argon, vacuum, and water vapor at room temperature. For tests in dehumified argon, the environment was maintained around the crack by flowing argon (purified by a suitable purification system) through chambers clamped to the faces of the specimen [21]. Tests in vacuum and in water vapor were carried out inside a commercial ultra-high vacuum chamber that had been modified to provide mechanical force feed-throughs. Tests in vacuum were made at pressures below 0.50 μPa. Water vapor was obtained by backfilling the chamber from a high-purity source following bake-out of the system. Pressure was monitored by a capacitance manometer, and purity was checked with the aid of a quadrupole residual gas analyzer.

Experimental Procedures

The fatigue crack growth experiments were carried out under constant amplitude loading in a closed-loop electrohydraulic testing machine operated in load control at a load ratio (R) of 0.05. Load control was estimated to be better than ± 1 pct. For the tests in argon, a frequency of 20 Hz was used. Tests in vacuum and in water vapor were carried out at 5 Hz.

Crack Monitoring System

An ac electrical potential system was used for monitoring crack growth [22-24]. For the specimen geometry, analytical relationships between crack length and electrical potential were not available, and calibration had to be established experimentally. Calibration was accomplished either by making simultaneous visual and electrical potential measurements of crack length on specimens fatigued in air, or by comparing electrical potential measurements

against fatigue markings on fracture surfaces produced by intentionally introduced high-load excursions (overloads) during fatigue in air [24].

Calibration results, given in terms of crack length (a) versus potential difference $(V-V_r)^{\dagger}$, can be represented by Eq. (2) [24].

$$a = 1.96 + 0.403\ (V - V_r) \quad (a \text{ in cm})$$

$$a = 0.77 + 0.159\ (V - V_r) \quad (a \text{ in in.}) \qquad (2)$$

$V = V(a)$ = potential corresponding to crack length a, and V_r = reference potential corresponding to the initial notch. Both V and V_r are given in microvolts. Accuracy of crack length measurement with the ac system was estimated to be better than 1 pct, for crack lengths from about 2 to 4.8 cm (0.8 to 1.85 in.). The resolution was better than 0.005 cm (0.002 in.) based on 12.5 nV resolution in electrical potential.

Fractography

Characterization of the morphology of fracture surfaces was made with the aid of scanning electron microscopy. Entire broken halves of the specimens were placed inside the microscope for examination. Specimen tilt was about an axis parallel to the direction of crack growth.

Surface Reactions

Auger electron spectroscopy (AES) and x-ray photoelectron spectroscopy (XPS)

---

†The electrical potential method provides measurements of crack length averaged through the thickness, while the visual method gives measurements of the crack length at the specimen surface only. Crack length measurements made by these two methods would differ because of crack front curvature. The discrepancy was significant for thick specimens. Corrections for crack front curvature were made by measuring average crack lengths from the fatigue markings (introduced during the calibration tests by changing the load amplitude) after specimen fracture. The average crack length was computed on the basis of five measurements - one at each specimen surface, one along each of the quarter-thickness planes and one along the mid-thickness plane. The "corrected" crack lengths are used in deriving Eq. (2) [24].

were used to determine the kinetics of the reactions of water vapor with 2219-T851 aluminum alloy surfaces [25]. For AES analyses, clean surfaces were produced by in situ impact fracture of notched round specimens. A polished and ion-etched alloy surface was used for the XPS analyses. Exposures of these clean surfaces to water vapor were achieved by back-filling the spectrometer chamber from a high purity source. High purity water vapor was obtained by alternately freezing and thawing triply distilled water, and pumping away the dissolved gases.

For these surface studies, background pressure in the spectrometer chamber was typically of the order of 6.7×10^{-2} μPa (5×10^{-10} torr), as measured on an ionization gage. The reactant gases were admitted into the chamber to pressures below 133 μPa (1×10^{-6} torr). The chamber was re-evacuated to below 0.67 μPa (5×10^{-9} torr) prior to each analysis. At these low pressures (< 133 μPa), reactions induced by species created by the ionization gage filament were minimal.

A different area of the impact fracture sample surface was analyzed by AES for each exposure, using a scanning Auger microprobe (SAM). For the XPS analyses, a freshly ion etched surface was used for each exposure. These procedures were followed to eliminate effects induced by the incident beam during previous measurements.

RESULTS

Fatigue Crack Growth Response

Room temperature fatigue crack growth data, obtained from tests in water vapor at pressures from 1 to 26.6 Pa (7.5×10^{-3} to 0.2 torr), are shown as a function of stress intensity factor range (ΔK) in Figure 1, along with data obtained from tests in dehumidified argon. The data at 26.6 Pa are comparable to those obtained in air (40 to 60 pct relative humidity), distilled water and

3.5 pct NaCl solution [24]. The results in dehumidified argon correspond to data in vacuum at less than 0.50 μPa ($\sim 4 \times 10^{-9}$ torr). These data are also shown in Figure 2 as a function of water vapor pressure at three ΔK levels. The error bands represent 95 pct confidence intervals computed from the residual standard deviations in each set of data [26,27]. The results show that, at a frequency of 5 Hz, the rate of crack growth is essentially unaffected by water vapor until a threshold pressure is reached. The rates then increased and reached a maximum within one order of magnitude increase in vapor pressure from this threshold. The maximum rate is equal to that obtained in air, distilled water and 3.5 pct NaCl solution (at 20 Hz) [24]. The transition range, in terms of pressure/frequency, is comparable to that reported by Bradshaw and Wheeler on another aluminum alloy [6].

Fractography

A photomacrograph of the fracture surface of a specimen tested in water vapor at 4.66 Pa (0.035 torr) is shown in Figure 3. This water vapor pressure corresponded to a position within the transition region in fatigue crack growth response (Figure 2). Principal interest here is in terms of the general features of the fracture surface morphology rather than with the details of the fracture processes. Examination of the photomacrograph indicates that the fracture surface appearance in the mid-thickness region differs considerably from that in the near-surface region. Scanning electron microfractographs taken from the same specimen indeed show differences in fracture surface morphology between the two regions, Figure 4. The fracture surface morphology may be compared with those observed on specimens tested in dehumidified argon and in water vapor at a pressure above the transition range, Figure 5. It is seen that the fracture morphology in the mid-thickness region (Figure 4a) is comparable to that associated with crack growth in dehumidified argon, an inert

environment, (Figure 5a), whereas the morphology in the near-surface region corresponds to that for full environmental effect (compare Figures 4b and 5b). This observation suggests that the effective water vapor pressure in the mid-thickness region of the crack may be substantially below that in the surrounding environment. The implication of this observation will be considered in the correlation of crack growth and surface reaction data.

Surface Reaction Kinetics

The results from AES and XPS studies of the reactions of water vapor and oxygen with clean surfaces of 2219-T851 aluminum alloy are presented in a companion paper [25]. A brief summary of those findings that bear directly on fatigue crack growth in water vapor is given here.

Changes in the normalized oxygen Auger (510 eV) signal as a function of exposure to water vapor are shown in Figure 6. Normalization is based on the average value of oxygen Auger (510 eV) signals from specimens exposed to water vapor for 6.65×10^{-2} to 1.33 Pa-s (5×10^{-4} to 10^{-2} torr-s). Comparable results were obtained from the XPS studies. The results show that the initial rate of reaction with water vapor is rapid and reaches "saturation" following about 2.7×10^{-3} Pa-s (2×10^{-5} torr-s) exposure; that is, the extent of reactions with water vapor is limited. XPS results indicate that the reactions are associated with the formation of an oxide or a hydrated oxide layer. The limited reactions with water vapor are consistent with previous results on a high-strength (AISI 4340) steel [16]. The rate of reaction with the aluminum alloy, however, is 8 to 9 orders of magnitude faster than the corresponding rate (associated with the slow, second step) of reaction with AISI 4340 steel. The surface reaction results will be considered in relation to environment assisted fatigue crack growth in the following discussion.

DISCUSSION

A comparison between the extent of surface reaction (Figure 6) and the fatigue crack growth response (Figure 2) may be made if one assumes that the enhancement of crack growth is proportional to the extent of surface reaction during one fatigue loading cycle [17,18], and if pressure/2 x frequency (p/2f) is used as an approximate measure of exposure*. This comparison shows that a factor of 10^3 adjustment in exposure (pt or p/2f) will have to be made to obtain a correlation. The need for this adjustment suggests that the rate of reaction at the crack tip is limited by the rate of transport of water vapor to that region. This possibility is also suggested by the differences in fracture surface morphology between the surface and mid-thickness regions of specimens tested within the transition region (i.e., between 0.13 and 1.3 Pa-s or 10^{-3} and 10^{-2} torr-s), and by the similarity between the observed morphology and the corresponding morphology for specimens tested in argon and at higher water vapor pressures (see Figures 3 to 5).

A transport limited model has been developed [18]. In this model, transport of gaseous environments to the crack tip is assumed to be by Knudsen flow [28]. The governing differential equations for flow and surface reactions are as follows [18]:

$$\frac{dp}{dt} = -\frac{SN_o RT}{V}\frac{d\theta}{dt} + \frac{F}{V}(p_o - p) \qquad (3)$$

$$\frac{d\theta}{dt} = k_c p(1-\theta) \qquad (4)$$

*It is assumed that the crack growth increment is introduced "abruptly" at the maximum load point in a given fatigue loading cycle. Thus, the newly produced crack surface is exposed to the environment only during one-half (unloading half) of the fatigue cycle.

The terms in the equations are as follows:

p = pressure of gas at the crack tip

p_o = pressure of gas in the surrounding environment

R = gas constant

S = area of newly created crack surface per cycle = α $(2B\Delta a)$, where Δa = crack growth increment per cycle, B = specimen thickness, and α = empirical constant for surface roughness and crack geometry [18]

T = absolute temperature

V = volume associated with the crack growth increment per cycle, i.e., with S

N_o = density of surface sites

θ = fractional surface coverage or extent of reaction of surface per unit area

$F = 8.72 \times 10^4 \beta \frac{\sigma_{ys}^2}{E^2} B\ell \left(\frac{T}{M}\right)^{1/2}$ (in cm^3/s) = Knudsen flow parameter that depends on dimension and shape of the capillary, molecular weight (M) of the gas and temperature (T). The specific form of this expression reflects an attempt to account for constriction in flow by the real crack, where ℓ is an arbitrary distance (of the order 10^{-4} cm) from the crack tip used in defining a crack opening and β is an empirical quantity to be determined from the crack growth data [18,28].

k_c = reaction rate constant

From Equation (3), it can be seen that the rate of change of pressure at the crack tip depends on the decrease in pressure produced by reaction of the environment with the newly created crack surface and on the increase in pressure from the influx of gas from the external environment. Equation (4) incorporates the

assumption that the surface reaction was first-order in relation to available surface sites [18,25,27]

Equations (3) and (4) are nonlinear, coupled equations which can be solved, at least in principle, for specific cases. Numerical solutions for these equations have been obtained using reasonable, assumed values for S and F and measured value for k_c [25]. These numerical results are illustrated in Figures 7 and 8. Figure 7 was derived by assuming the initial pressure to be zero at the crack tip, and shows that the percent attenuation in pressure is essentially independent of the external pressure. For Figure 8, the initial pressure at the crack tip was assumed to be equal to the external pressure. It is seen that the pressure decreased rapidly and reached an attenuated value that is essentially the same as the previous case. In either case, the attenuated pressure was more than two orders of magnitude lower than the external pressure, and remained nearly constant as long as the crack surface remained active. The surface coverage (or extent of surface reaction) increased almost linearly with time; the rate of increase being proportional to the local pressure at the crack tip. This transport-limited change in surface coverage would provide much better agreement with the fatigue data.

To provide for a more formal comparison, Equations (3) and (4) may be solved approximately. By combining Equations (3) and (4), one can obtain an expression for the pressure at the crack tip.

$$p = \frac{p_o - \frac{Vdp}{Fdt}}{\frac{SN_o RTk_c}{F}(1-\theta) + 1} \qquad (5)$$

It has been shown that the term (V/F)(dp/dt) may be neglected in comparison with p_o during the reaction, except at the very beginning of the reaction (or for $\theta \approx 0$) [18]. Using this simplifying assumption, Equation (4) may be rewritten as

$$\frac{d\theta}{dt} = k_c p(1-\theta) = \frac{k_c p_o (1-\theta)}{\frac{SN_o RTk_c}{F}(1-\theta) + 1} \tag{6}$$

Integration of Equation (6) gives the surface coverage θ as a function of $p_o t$

$$\frac{SN_o RT}{F}\theta - \frac{1}{k_c}\ell n(1-\theta) = p_o t \tag{7}$$

For this 2219-T851 aluminum alloy tested in water vapor, $SN_o RT/F$ is estimated to be of the order 1 Pa-s and k_c is of the order 10^3 $(Pa\text{-}s)^{-1}$ [25]. In other words, $SN_o RTk_c/F$ is of the order 10^3. Thus, the reactions at the crack tip are limited by flow and θ may be described adequately by the linear term alone up to $\theta \approx 0.99$ for this case, that is

$$\theta \approx \frac{F}{SN_o RT} p_o t \tag{8}$$

If t is taken to be equal to $\tau/2$ or $1/2f$, then

$$\theta \approx 4.36 \times 10^4 \frac{\beta}{\alpha} \frac{\sigma_{ys}^2 \ell}{N_o RTE^2} \left(\frac{T}{M}\right)^{1/2} \cdot \frac{p_o}{2f\Delta a} \tag{9}$$

In other words, the extent of reaction, as measured by θ, during a cycle is proportional to p_o, and is inversely proportional to frequency and the extent of crack growth (Δa) during that cycle, up to $\theta \approx 1$. With further increase in pressure or decrease in frequency, θ should remain at 1, i.e., at saturation coverage. It has been suggested that the rate of environment assisted fatigue crack growth, $(da/dN)_e$, may be considered to be the sum of two components -- the rate of growth in an inert reference environment or "pure fatigue", $(da/dN)_r$, and the environmental or "corrosion fatigue" component, $(da/dN)_{cf}$ [29]. The growth increment per cycle (Δa) is therefore identified with $(da/dN)_e \cdot (1)$. The environmental component is considered to be a function of the amount of hydrogen that is produced (or extent of reaction) during one cycle, and should be proportional to $\Delta a \cdot \theta$, and the number of hydrogen atoms produced

per water molecule reaction. Thus, one can expect $(da/dN)_{cf}$ to vary according to Equation (10) for $\theta<1.0$.

$$\left(\frac{da}{dN}\right)_{cf} = \left(\frac{da}{dN}\right)_e - \left(\frac{da}{dN}\right)_r \propto 4.36 \times 10^4 \frac{\beta}{\alpha} \frac{\sigma_{ys}^2 \ell}{N_o RTE^2} \left(\frac{T}{M}\right)^{1/2} \frac{p_o}{2f} \qquad (10)$$

For combinations of p_o and f values that would yield $\theta \to 1$, $(da/dN)_{cf}$ and $(da/dN)_e$ would represent maximum enhancement that can be achieved.

Comparison of Equation (10) with fatigue crack growth data is shown in Figure 9. Data at three different ΔK levels are used, and are normalized with respect to the average of $(da/dN)_{cf}$ values for water vapor at 6.9 and 26.6 Pa, air, distilled water and 3.5 pct NaCl solution at each ΔK level. These average values are used to represent the "saturation" values of $(da/dN)_{cf}$. Because $(da/dN)_{cf}$ represents the difference between $(da/dN)_e$ and $(da/dN)_r$, errors tend to be very large, particularly at the lower water vapor pressures. Estimates of error were computed from the residual standard deviations in each set of data, and are shown in Figure 9. The data indicate the desired linear dependence on p_o or $p_o/2f$ below "saturation", and suggest that the pressure needed to produce "saturation" is essentially independent of ΔK. The latter observation suggests that the characteristic length ℓ in Equation (10) depends on ΔK. If one assumes ℓ to be equal to the growth increment per cycle at "saturation", then the data can be matched to Equation (10) to determine the empirical constants β/α. Alternatively, β/α may be determined from the observed pressure at the onset of saturation response and Equation (9), i.e., for $\theta \approx 1$, using the same assumption. The value of β/α was found to be approximately equal to 1.5. The fitted curves, based on Equation (10), are shown in both Figures 2 and 9, and show good agreement with the data.

If one takes $\alpha = 2$ as a reasonable estimate of the contributions of crack shape and surface roughness to the crack area, then $\beta = 3$. If one now assigns

β to the constricted flow length, this length is estimated to be approximately equal to $2r_y$ (where $r_y = \frac{1}{2\pi}(K/\sigma_{ys})^2$ is the formally calculated plastic zone correction factor), or equal to about 0.07 cm at K_{max} = 16.5 MPa-$m^{1/2}$. The estimated effective crack opening at this K_{max} is about 4×10^{-5} cm. Alternatively, one may assign β to the effective crack opening, thus providing a constricted flow length of about 0.2 cm and an effective opening of 7×10^{-5} cm. These quantities appear to be quite reasonable in either case. Thus, a satisfactory fracture mechanics and surface chemistry explanation of the observed fatigue crack growth response has been achieved.

Examination of Equations (5) and (6) shows that if $SN_0RTk_c/F \ll 1$, that is for low k_c or "slow" reaction kinetics, the pressure at the crack tip becomes equal to the external pressure following a fast initial build up, and surface reaction is now limited by the surface reaction kinetics. This latter case is consistent with previous observations on AISI 4340 steel in water vapor [17]. The observed difference in fatigue crack growth response and a factor of 10^8 to 10^9 difference in reaction rate constants for aluminum alloys and steel with water vapor [16,25], are consistent with these observations.

The fact that no further increase in the rate of fatigue crack growth for this aluminum alloy was observed in the aqueous environments over that in water vapor at "saturation" is consistent with the observation that the aluminum-water reaction is limited [25]. It also suggests that enhancement of crack growth results from hydrogen embrittlement vis-a-vis active path dissolution. The precise mechanics for this hydrogen embrittlement remains to be identified. The fact that significant environment enhancement of crack growth can occur in fatigue in aluminum alloys, as opposed to sustained-load crack growth, resides with the efficiency of the fatigue process in creating "fresh" surfaces to react with the environment.

SUMMARY

Coordinated fracture mechanics and surface chemistry studies were carried out to develop further understanding of the influence of water vapor on fatigue crack growth in aluminum alloys. The results confirm the earlier suggestion by Bradshaw and Wheeler that the enhancement of crack growth is a function of water vapor pressure and the time available for reaction, that is, of exposure (pressure x time). The enhancement is shown to be dependent on the rate of transport of water vapor to the crack tip, as well as on the surface reaction kinetics. The results also suggest that hydrogen produced by the surface reactions is responsible for the enhancement in growth, vis-a-vis an active path dissolution mechanism. The observed fatigue crack growth response is adequately described in terms of a transport-limited model for fatigue crack growth.

ACKNOWLEDGEMENT

Support of this research by the Office of Naval Research under Contract N00014-75-C-0543, NR 036-097, and through Faculty Research Grants from the ALCOA Foundation is gratefully acknowledged. The authors also express their appreciation to Messrs. R. Brazill and C. D. Miller for their assistance with the fracture mechanics experiments.

REFERENCES

1. R. P. Wei: J. Engr. Fract. Mech, 1, p. 633, 1970.

2. A. J. McEvily and R. P. Wei: Corrosion Fatigue, ed. O. Devereux, A. J. McEvily and R. W. Staehle, NACE, Houston, Texas, p. 381, 1972.

3. Corrosion Fatigue, NACE, Houston, Texas, 1972.

4. Fatigue Crack Propagation, ASTM STP 415, Am. Soc. Testing Matls., Philadelphia, Pennsylvania, 1967.

5. R. P. Wei and M. O. Speidel: Corrosion Fatigue, ed. O. Devereux, A. J. McEvily and R. W. Staehle, NACE, Houston, Texas, p. 379, 1972.

6. F. J. Bradshaw and C. Wheeler: Int. J. Fract. Mech., 5, pp. 255-268, Dec., 1969.

7. A. Hartman, F. J. Jacobs, A. Nederveen and R. DeRijk: NLR Tech. Note No. M2181, 1967.

8. R. P. Wei: Int. J. Fract. Mech., 4, p. 159, 1968.

9. S. J. Hudak and R. P. Wei: Corrosion Fatigue, ed. O. Devereux, A. J. McEvily and R. W. Staehle, NACE, Houston, Texas, p. 433, 1972.

10. R. P. Wei and J. D. Landes: Matls. Res. Std., 9, p. 25, 1969.

11. J. M. Barsom: Corrosion Fatigue, ed. O. Devereux, A. J. McEvily and R. W. Staehle, NACE, Houston, Texas, p. 424, 1972.

12. J. P. Gallagher and R. P. Wei: Corrosion Fatigue, ed. O. Devereux, A. J. McEvily and R. W. Staehle, NACE, Houston, Texas, p. 409, 1972.

13. G. A. Miller, S. J. Hudak and R. P. Wei: J. Testing and Evaluation, 1, p. 524, 1973.

14. J. P. Hutin: M.S. Thesis, Lehigh University, 1975.

15. D. J. Dwyer, G. W. Simmons and R. P. Wei: Surf. Sci., 64, pp. 617-632, 1977.

16. G. W. Simmons, P. S. Pao and R. P. Wei: Met. Trans. A, 9A, pp. 1147-1158, 1978.

17. P. S. Pao, W. Wei and R. P. Wei: "Effect of Frequency on Fatigue Crack Growth Response of AISI 4340 Steel in Water Vapor", TMS-AIME, in press.

18. T. W. Weir, R. G. Hart, G. W. Simmons and R. P. Wei: "A Flow Limited Model for Environment Assisted Fatigue Crack Growth", to be published.

19. Wilson, W. K.: Westinghouse Research Laboratories, Report No. WERL-0029-3, 1965.

20. Wilson, W. K.: Westinghouse Research Laboratories, Report No. 66-1B4-BTLFR-R1, 1966.

21. R. P. Gangloff and R. P. Wei: Fractography in Failure Analysis, ASTM STP 645, ed. B. M. Strauss and W. H. Cullen, Jr., pp. 87-106, 1978.

22. H. H. Johnson: Matls. Res. Std., 6, p. 422, 1966.

23. Che-Yu Li and R. P. Wei: Matls. Res. Std., 6, p. 392, 1966.

24. R. P. Wei and N. E. Fenelli: "Fatigue Crack Growth Response Following a High-Load Excursion in 2219-T851 Aluminum Alloy", to be published.

25. R. G. Hart, G. W. Simmons and R. P. Wei: "AES and XPS Studies of the Reactions of Oxygen and Water Vapor With an Aluminum Alloy", to be published.

26. W. G. Clark, Jr. and S. J. Hudak, Jr.: J. Testing and Evaluation, 3, No. 6, pp. 454-476, Nov., 1975.

27. R. P. Wei, W. Wei and G. A. Miller: J. Testing and Evaluation, 7, No. 2, pp. 90-95, March, 1979.

28. S. Dushman: Scientific Foundations of Vacuum Technique, 2nd Edition, ed. J. M. Lafferty, Wiley, p. 88, 1962.

29. R. P. Wei: "On Understanding Environment Enhanced Fatigue Crack Growth - A Fundamental Approach", Fatigue Mechanisms, Proceedings of an ASTM-NBS-NSF symposium, Kansas City, Mo., May 1978, ed. J. T. Fong, ASTM-STP 675, 1979, in press.

FIGURE CAPTIONS

Figure 1: Influence of water vapor pressure on the kinetics of fatigue crack growth in 2219-T851 aluminum alloy at room temperature.

Figure 2: Influence of water vapor pressure (or $^{\text{pressure}}/_{2\text{xfrequency}}$) on fatigue crack growth rates in 2219-T851 aluminum alloy at room temperature. Solid lines represent model predictions.

Figure 3: Photo-macrograph of fatigue fracture surface of 2219-T851 aluminum alloy specimen tested in water vapor (4.66 Pa) at room temperature. (ΔK = 16.5 MPa-$m^{1/2}$, R = 0.05 and f = 5 Hz).

Figure 4: SEM microfractographs taken from the mid-thickness region (center) and the near-surface region (edge) of the specimen shown in Figure 3 showing differences in fracture surface morphology.

Figure 5: SEM microfractographs of specimens tested in argon and in water vapor at 26.6 Pa (full environmental effect) showing similar differences in fracture surface morphology as seen in Figure 4.

Figure 6: Kinetics of reactions of water vapor with 2219-T851 aluminum alloy at room temperature [25].

Figure 7: Variation of water vapor pressure and surface coverage at the crack tip as a function of time, assuming that the initial pressure at the crack tip is zero (p_i = 0) [18].

Figure 8: Variation of water vapor pressure and surface coverage at the crack tip as a function of time, assuming that the initial pressure at the crack tip is equal to the external pressure ($p_i = p_o$) [18].

Figure 9: Comparison of normalized (corrosion) fatigue crack growth rates with model predictions for pressure and frequency dependence.

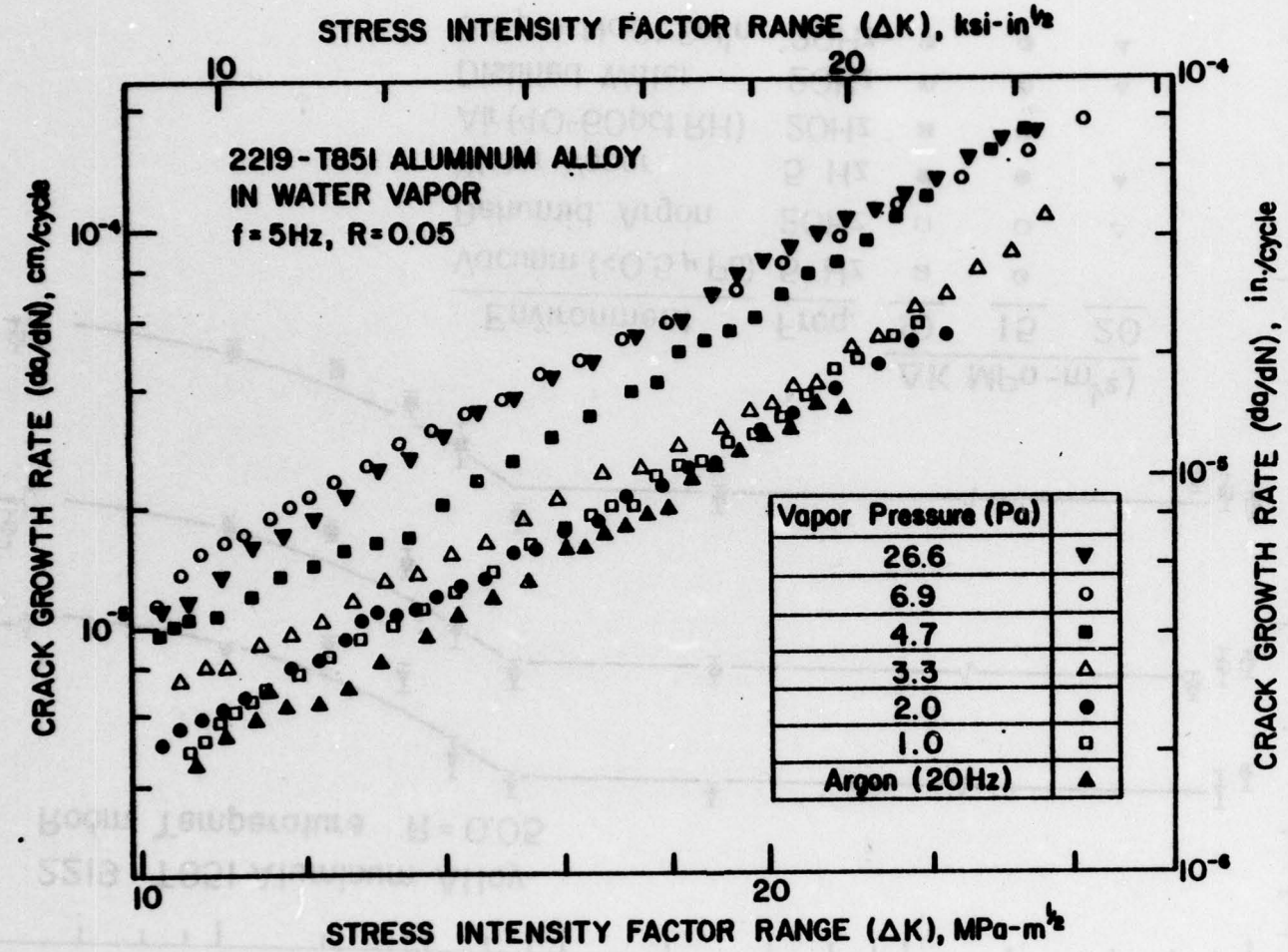

Figure 1: Influence of water vapor pressure on the kinetics of fatigue crack growth in 2219-T851 aluminum alloy at room temperature.

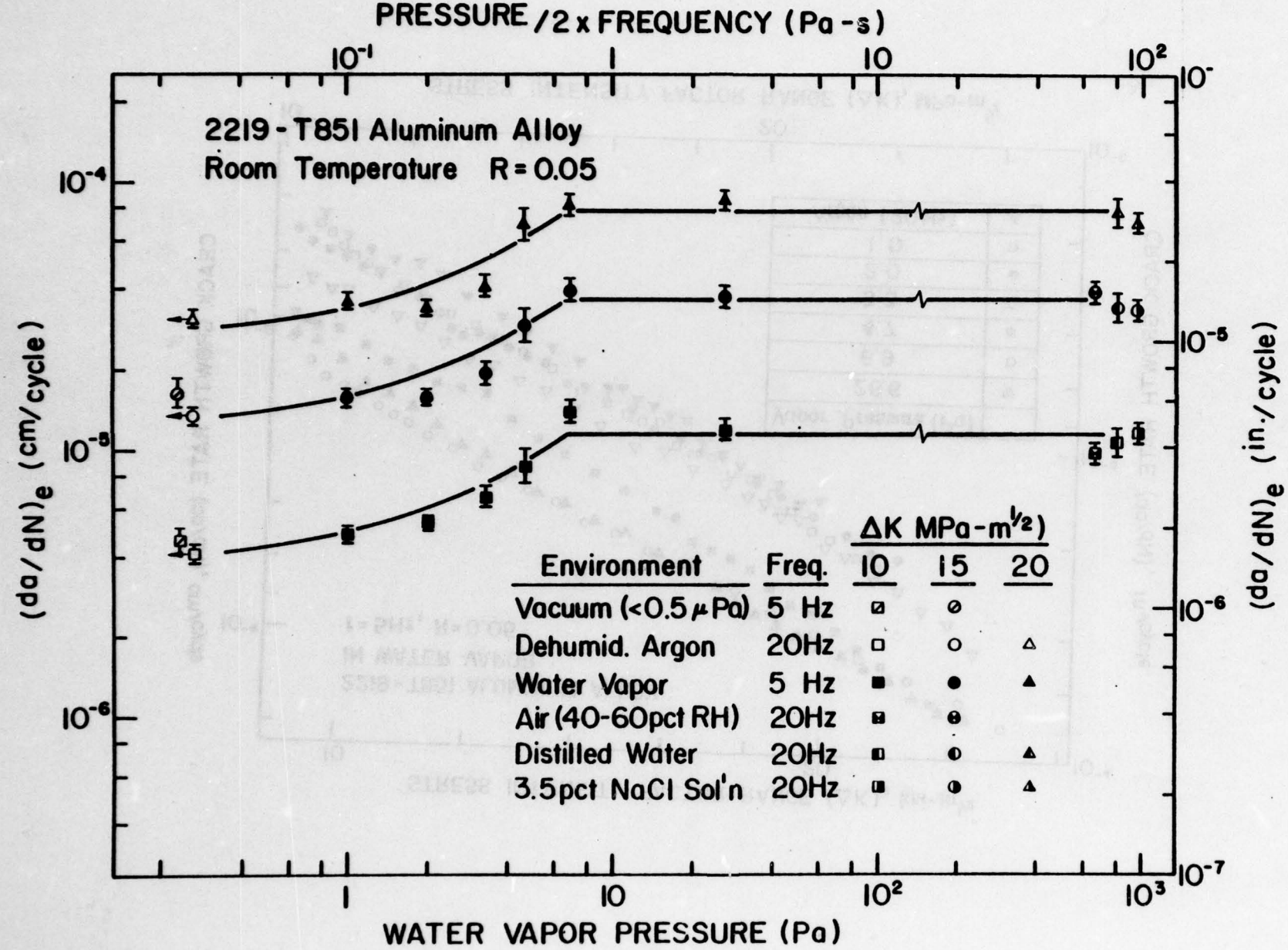

Figure 2: Influence of water vapor pressure (or pressure/2xfrequency) on fatigue crack growth rates in 2219 T851 aluminum alloy at room temperature. Solid lines represent model pre-

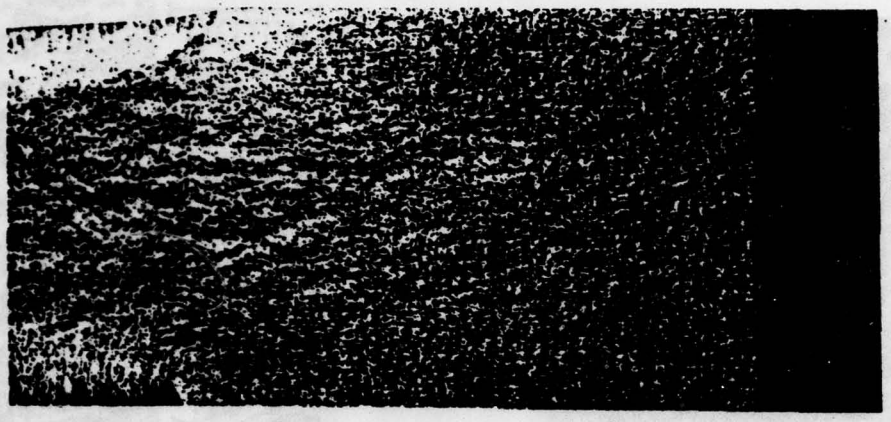

Figure 3: Photo-macrograph of fatigue fracture surface of 2219-T851 aluminum alloy specimens tested in water vapor (4.66 Pa) at room temperature. (ΔK = 16.5 MPa-$m^{1/2}$, R = 0.05 and f = 5 Hz).

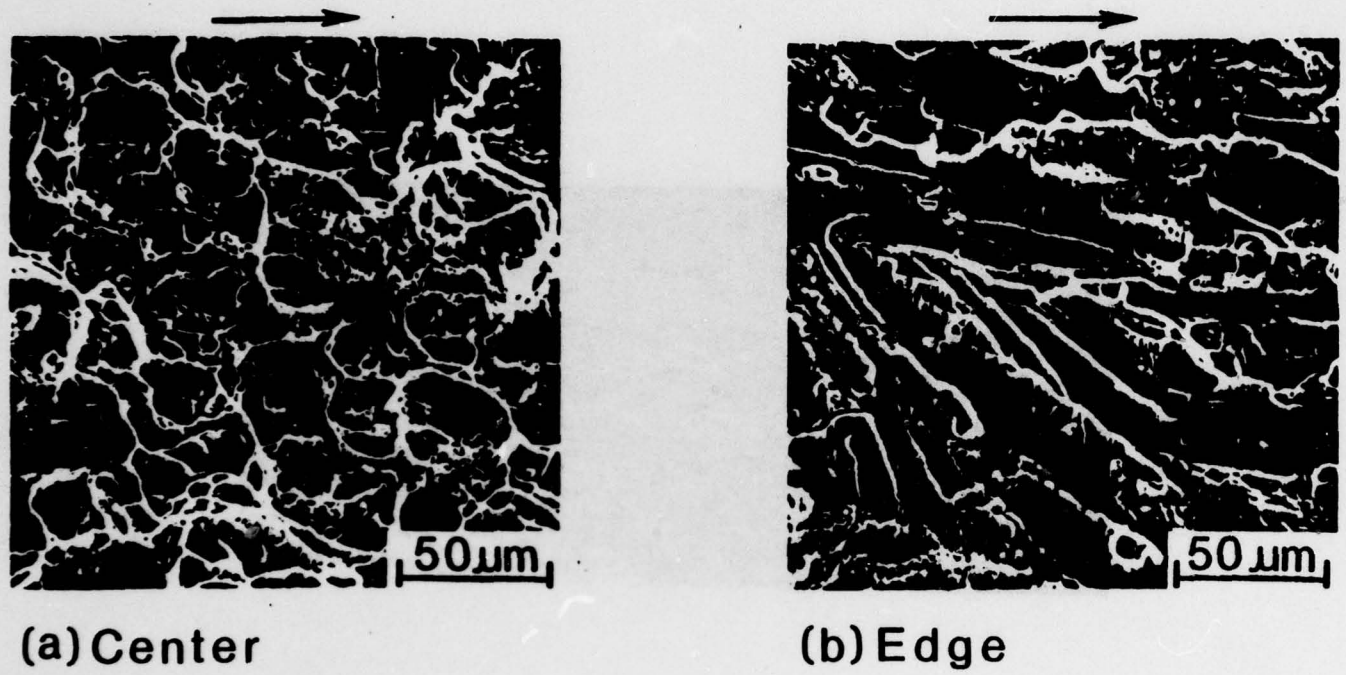

Figure 4: SEM microfractographs taken from the mid-thickness region (center) and the near-surface region (edge) of the specimen shown in Figure 3 showing differences in fracture surface morphology.

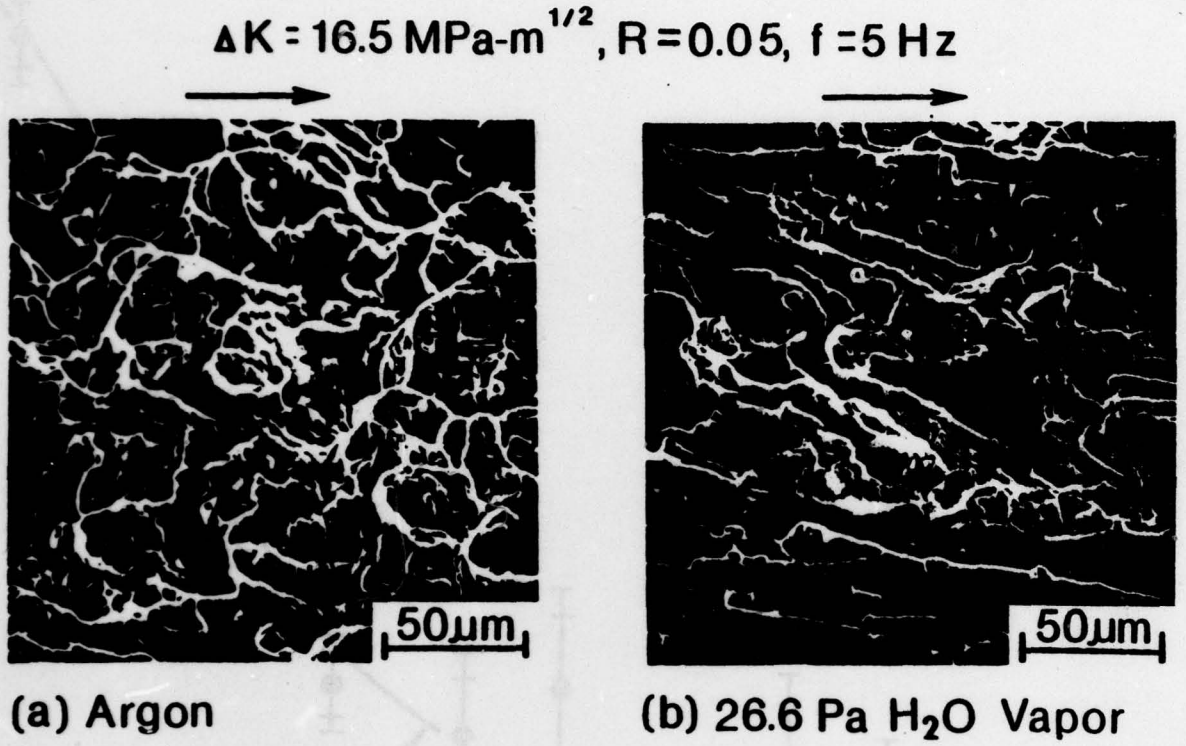

Figure 5: SEM microfractographs of specimens tested in argon and in water vapor at 26.6 Pa (full environmental effect) showing similar differences in fracture surface morphology as seen in Figure 4.

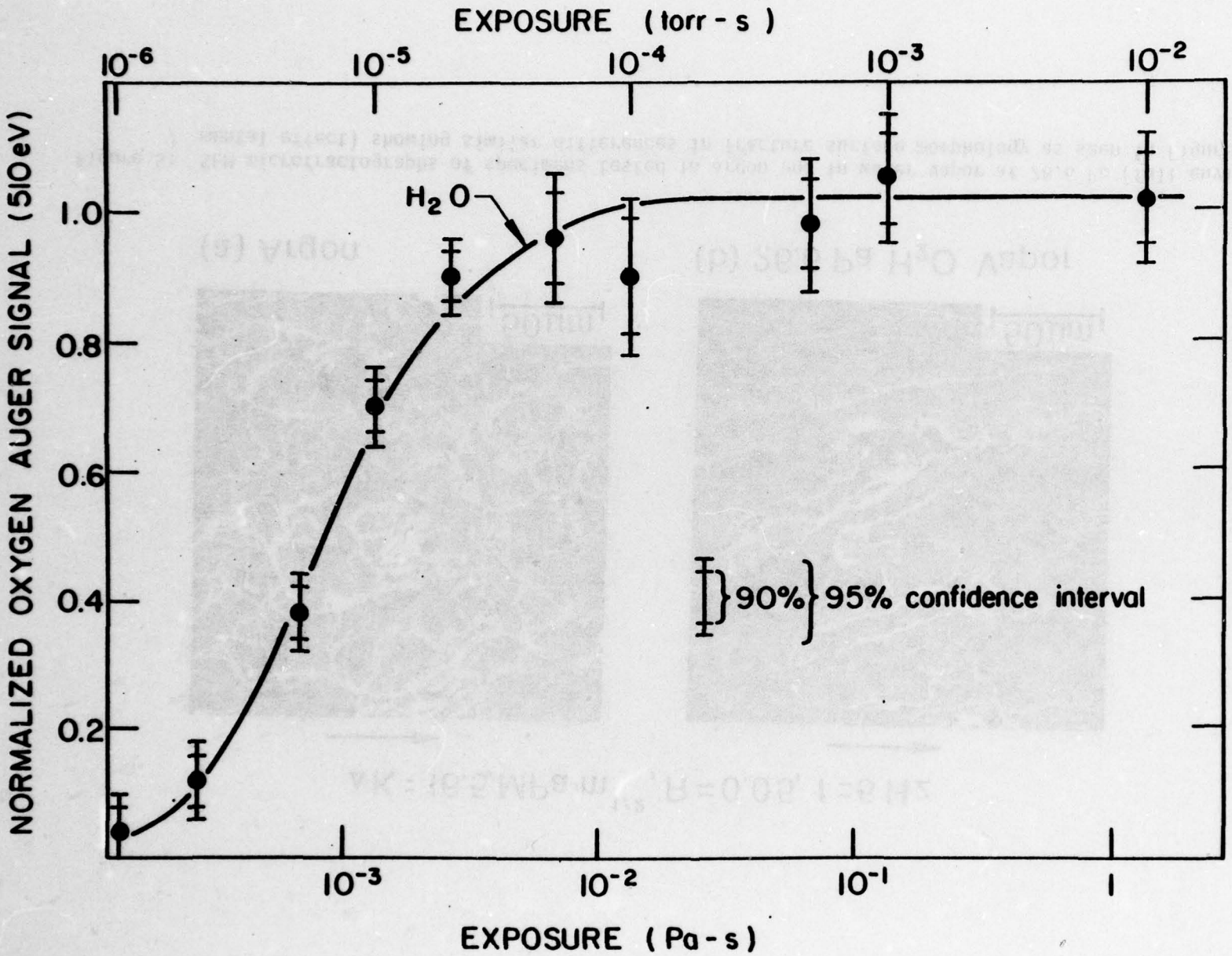

Figure 6: Kinetics of reactions of water vapor with 2219 T851 aluminum alloy at room [illegible]

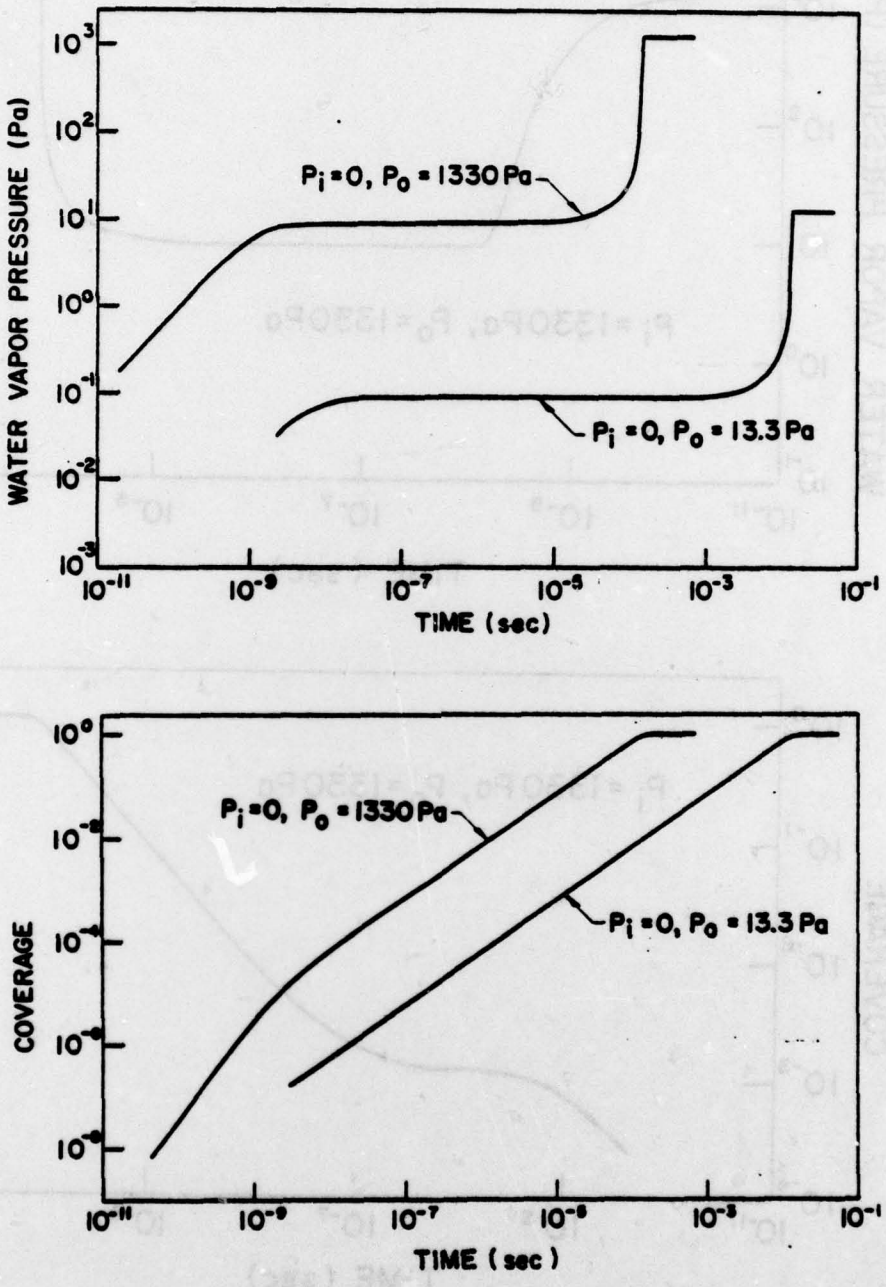

Figure 7: Variation of water vapor pressure and surface coverage at the crack tip as a function of time, assuming that the initial pressure at the crack tip is zero ($p_i = 0$) [18].

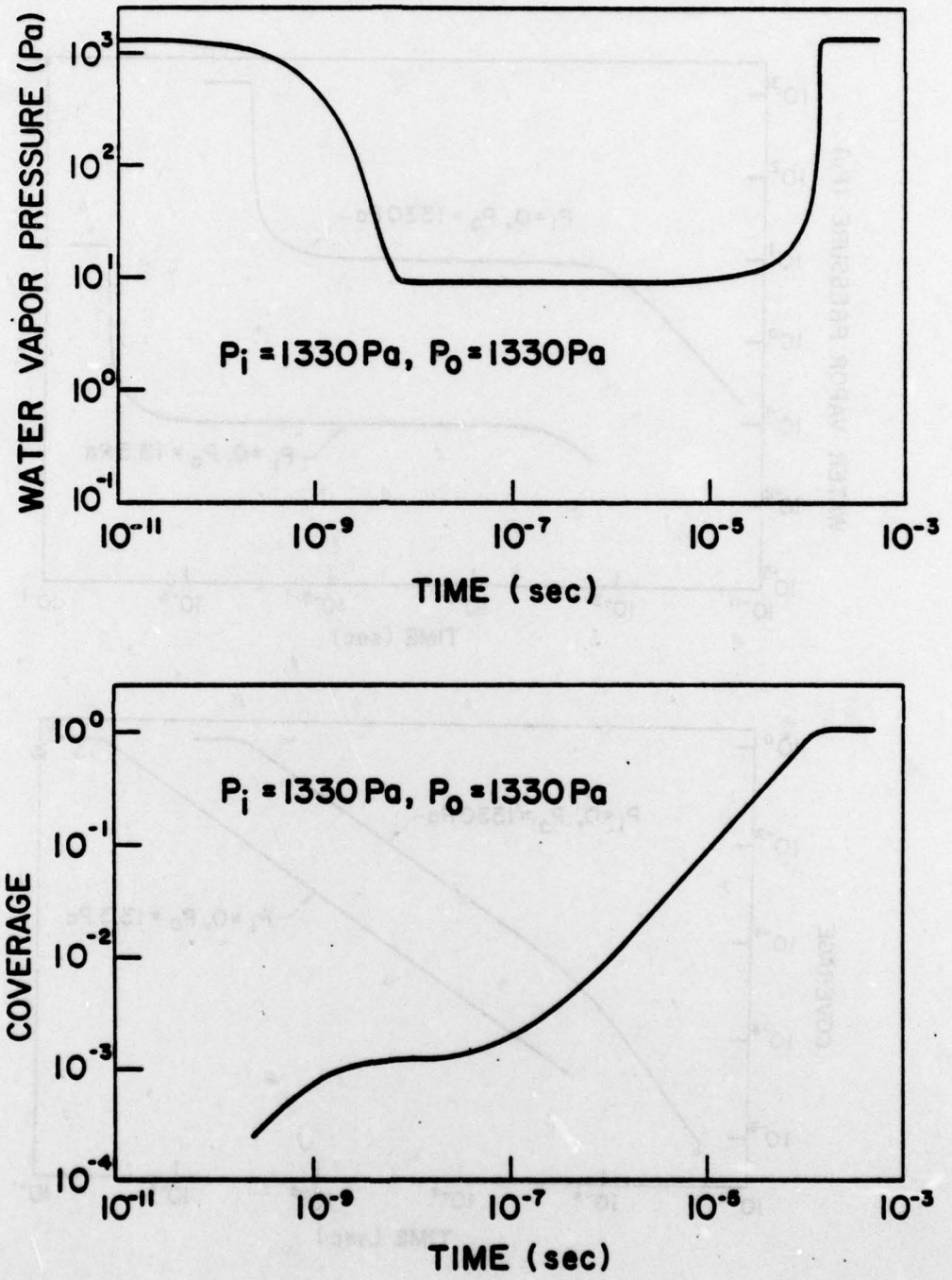

Figure 8: Variation of water vapor pressure and surface coverage at the crack tip as a function of time, assuming that the initial pressure at the crack tip is equal to the external pressure ($p_i = p_0$) [18].

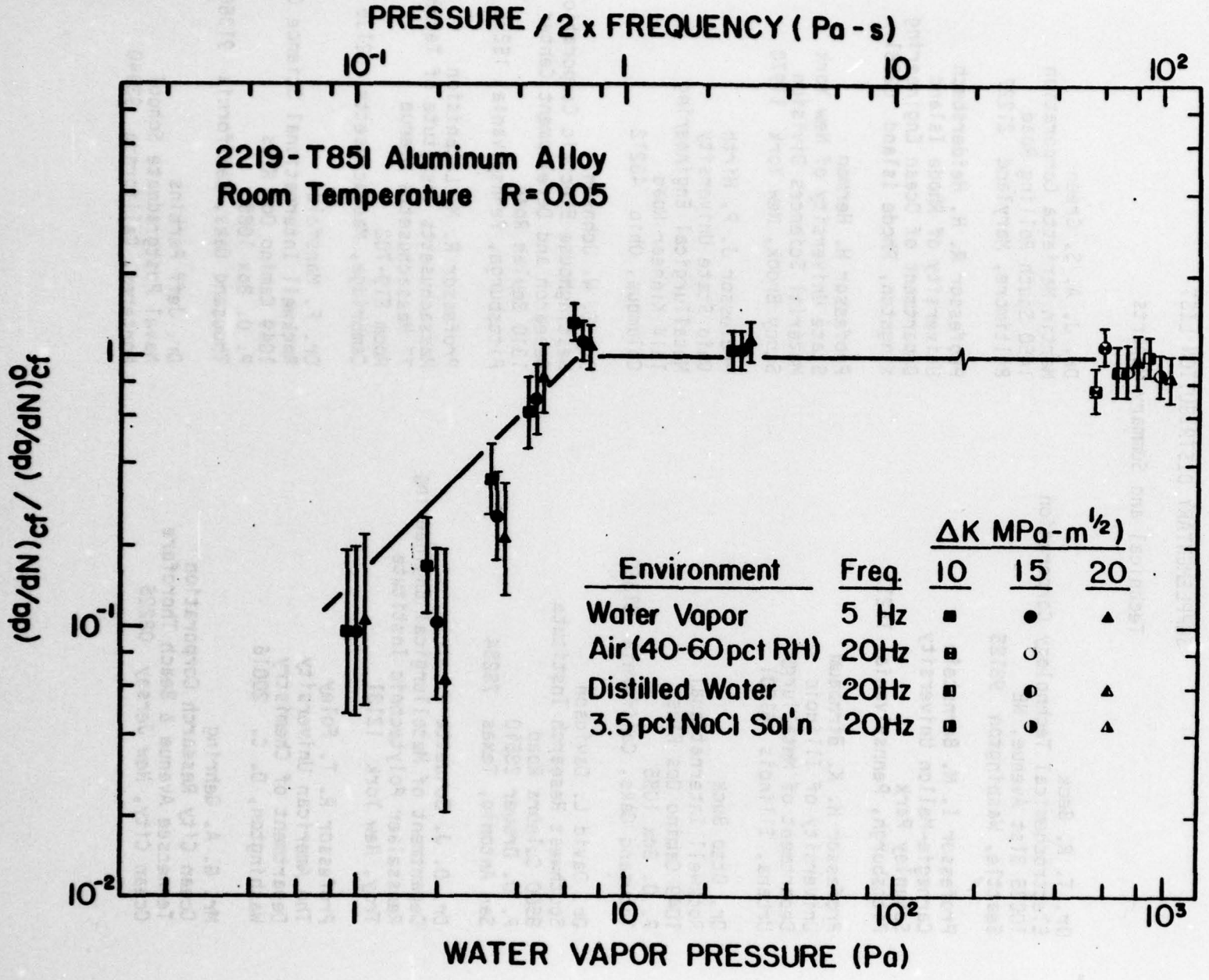

Figure 9: Comparison of normalized (corrosion) fatigue crack growth rates with model predictions for pressure and frequency dependence.

C
January 1979

SUPPLEMENTARY DISTRIBUTION LIST

Technical and Summary Reports

Dr. T. R. Beck
Electrochemical Technology Corporation
10035 31st Avenue, NE
Seattle, Washington 98125

Professor I. M. Bernstein
Carnegie-Mellon University
Schenley Park
Pittsburgh, Pennsylvania 15213

Professor H. K. Birnbaum
University of Illinois
Department of Metallurgy
Urbana, Illinois 61801

Dr. Otto Buck
Rockwell International
1049 Camino Dos Rios
P. O. Box 1085
Thousand Oaks, California 91360

Dr. David L. Davidson
Southwest Research Institute
8500 Culebra Road
P. O. Drawer 28510
San Antonio, Texas 78284

Dr. D. J. Duquette
Department of Metallurgical Engineering
Rensselaer Polytechnic Institute
Troy, New York 12181

Professor R. T. Foley
The American University
Department of Chemistry
Washington, D. C. 20016

Mr. G. A. Gehring
Ocean City Research Corporation
Tennessee Avenue & Beach Thorofare
Ocean City, New Jersey 08226

Dr. J. A. S. Green
Martin Marietta Corporation
1450 South Rolling Road
Baltimore, Maryland 21227

Professor R. H. Heidersbach
University of Rhode Island
Department of Ocean Engineering
Kingston, Rhode Island 02881

Professor H. Herman
State University of New York
Material Sciences Division
Stony Brook, New York 11970

Professor J. P. Hirth
Ohio State University
Metallurgical Engineering
1314 Kinnear Road
Columbus, Ohio 43212

Dr. E. W. Johnson
Westinghouse Electric Corporation
Research and Development Center
1310 Beulah Road
Pittsburgh, Pennsylvania 15235

Professor R. M. Latanision
Massachusetts Institute of Technolog
77 Massachusetts Avenue
Room E19-702
Cambridge, Massachusetts 02139

Dr. F. Mansfeld
Rockwell International Science Cente
1049 Camino Dos Rios
P. O. Box 1085
Thousand Oaks, California 91360

Dr. Jeff Perkins
Naval Postgraduate School
Monterey, California 93940

C
January 1979

SUPPLEMENTARY DISTRIBUTION LIST
(Continued)

Professor H. W. Pickering
Pennsylvania State University
Department of Material Sciences
University Park, Pennsylvania 16802

Dr. E. A. Starke, Jr.
Georgia Institute of Technology
School of Chemical Engineering
Atlanta, Georgia 30332

Dr. Barry C. Syrett
Stanford Research Institute
333 Ravenswood Avenue
Menlo Park, California 94025

Dr. R. P. Wei
Lehigh University
Institute for Fracture and
Solid Mechanics
Bethlehem, Pennsylvania 18015

Professor H. G. F. Wilsdorf
University of Virginia
Department of Materials Science
Charlottesville, Virginia 22903

Dr. Clive Clayton
State University of New York
Material Sciences Division
Stony Brook, New York 11970

BASIC DISTRIBUTION LIST

Technical and Summary Reports April 1978

Organization	Copies
Defense Documentation Center Cameron Station Alexandria, VA 22314	12
Office of Naval Research Department of the Navy 800 N. Quincy Street Arlington, VA 22217	
ATTN: Code 471	1
Code 102	1
Code 470	1
Commanding Officer Office of Naval Research Branch Office Building 114, Section D 666 Summer Street Boston, MA 02210	1
Commanding Officer Office of Naval Research Branch Office 536 South Clark Street Chicago, IL 60605	1
Office of Naval Research San Francisco Area Office One Hallidie Plaza Suite 601 San Francisco, CA 94102	1
Naval Research Laboratory Washington, DC 20375	
ATTN: Codes 6000	1
6100	1
6300	1
6400	1
2627	1
Naval Air Development Center Code 302 Warminster, PA 18964 ATTN: Mr. F. S. Williams	1

Organization	Copies
Naval Air Propulsion Test Center Trenton, NJ 08628 ATTN: Library	1
Naval Construction Batallion Civil Engineering Laboratory Port Hueneme, CA 93043 ATTN: Materials Division	1
Naval Electronics Laboratory San Diego, CA 92152 ATTN: Electron Materials Sciences Division	1
Naval Missile Center Materials Consultant Code 3312-1 Point Mugu, CA 92041	1
Commanding Officer Naval Surface Weapons Center White Oak Laboratory Silver Spring, MD 20910 ATTN: Library	1
David W. Taylor Naval Ship Research and Development Center Materials Department Annapolis, MD 21402	1
Naval Undersea Center San Diego, CA 92132 ATTN: Library	1
Naval Underwater System Center Newport, RI 02840 ATTN: Library	1
Naval Weapons Center China Lake, CA 93555 ATTN: Library	1
Naval Postgraduate School Monterey, CA 93940 ATTN: Mechanical Engineering Department	1

BASIC DISTRIBUTION LIST (cont'd)

Organization	Copies
Naval Air Systems Command Washington, DC 20360 ATTN: Codes 52031 52032	1
Naval Sea System Command Washington, DC 20362 ATTN: Code 035	1
Naval Facilities Engineering Command Alexandria, VA 22331 ATTN: Code 03	1
Scientific Advisor Commandant of the Marine Corps Washington, DC 20380 ATTN: Code AX	1
Naval Ship Engineering Center Department of the Navy Washington, DC 20360 ATTN: Code 6101	1
Army Research Office P.O. Box 12211 Triangle Park, NC 27709 ATTN: Metallurgy & Ceramics Program	1
Army Materials and Mechanics Research Center Watertown, MA 02172 ATTN: Research Programs Office	1
Air Force Office of Scientific Research Bldg. 410 Bolling Air Force Base Washington, DC 20332 ATTN: Chemical Science Directorate	1
Electronics & Solid State Sciences Directorate	1
Air Force Materials Laboratory Wright-Patterson AFB Dayton, OH 45433	1
Library Building 50, Rm 134 Lawrence Radiation Laboratory Berkeley, CA	1

Organization	Copies
NASA Headquarters Washington, DC 20546 ATTN: Code RRM	1
NASA Lewis Research Center 21000 Brookpark Road Cleveland, OH 44135 ATTN: Library	1
National Bureau of Standards Washington, DC 20234 ATTN: Metallurgy Division	1
Inorganic Materials Div.	1
Director Applied Physics Laboratory University of Washington 1013 Northeast Forthieth Street Seattle, WA 98105	1
Defense Metals and Ceramics Information Center Battelle Memorial Institute 505 King Avenue Columbus, OH 43201	1
Metals and Ceramics Division Oak Ridge National Laboratory P.O. Box X Oak Ridge, TN 37380	1
Los Alamos Scientific Laboratory P.O. Box 1663 Los Alamos, NM 87544 ATTN: Report Librarian	1
Argonne National Laboratory Metallurgy Division P.O. Box 229 Lemont, IL 60439	1
Brookhaven National Laboratory Technical Information Division Upton, Long Island New York 11973 ATTN: Research Library	1
Office of Naval Research Branch Office 1030 East Green Street Pasadena, CA 91106	1